

Chapter 9

Transverse Spherocity

In this chapter, measurements of K_S^0 , Λ , and $\bar{\Lambda}$ are reported as a function of transverse spherocity $S_O^{(p_T=1.0)}$, a measure of the event's topology in the transverse xy -plane.

9.1 Transverse spherocity

9.1.1 Motivation for studying event topology

As explained in Chapter X, there is overwhelming evidence that some phenomena associated with QGP, such as collective flow and strangeness enhancement, also arise in pp and p–A collisions at LHC energies and high event multiplicities. This challenges the conventional assumption that the hadron densities and densities of colour fields between partons are too low to interact with each other. Consequently, high-multiplicity pp (and p–A) collisions cannot be treated as a superposition of mostly independent parton-parton (or parton-hadron) scatterings and a more in-depth approach is required to fully understand these phenomena.

Event shape observables have been used historically in lepton experiments to study fundamental QCD properties such as the gluon spin? , and also at Tevatron and the LHC in events with very high p_T ($\gtrsim 100$ GeV/c) jets to further test pQCD predictions? . There are various observables, including sphericity, spherocity, thrust, F-parameter, and Ellis-Karliner angle, most of which are collinear- and infrared-safe and therefore moderately easily calculable? . An illustration of two events with different topologies and calculated values of selected observables can be seen in Fig. 9.1.

With the discoveries of QGP phenomena in high-multiplicity collisions of small sys-

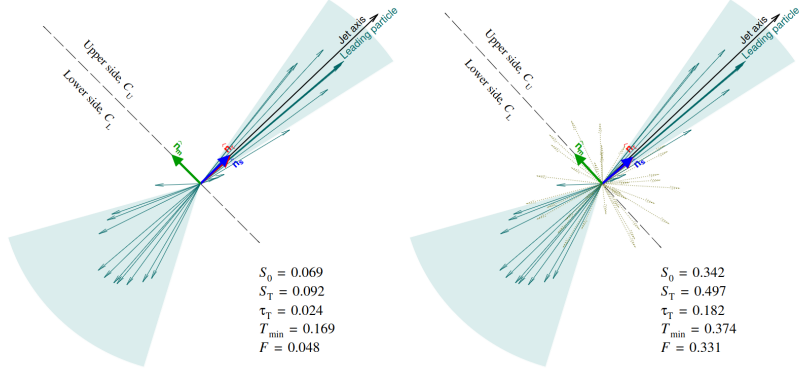


Figure 9.1: TBA.

tems, event shape observables become attractive for different reasons. This is because pQCD (“hard”) processes are responsible for a significant fraction of particle production and are likely to impact the character of QGP phenomena in non-trivial ways. The role of non-perturbative (“soft”) processes is particularly interesting to study as their mechanisms are not fully understood and their interpretation relies on phenomenological models that require clear experimental measurements with high discriminatory power.

Event shape observables allow us to quantify events according to the dominant contributing processes. For instance, collisions with single large p_T transfer scatterings are likely to lead into events with two back-to-back, highly collimated showers, which create a pencil-like shape in the transverse plane. Conversely, collisions with multiple lower p_T transfer partonic interactions will exhibit a high degree of azimuthal isotropy. Therefore, event shape measurements help us gain a deeper understanding of high-multiplicity events and a better control over the magnitudes of the hard and soft contributions. Ultimately, these measurements may help determine whether QGP formation is necessary in small systems or uncover new physical behaviours.

9.1.2 S_O and $S_O^{(p_T=1.0)}$ as experimental observables

Traditionally, spherocity S_O is defined as:

$$S_O = \frac{\pi^2}{4} \min_{\hat{n}} \left(\frac{\sum_i |p_{T,i} \times \hat{n}|}{\sum_i |p_{T,i}|} \right)^2 , \quad (9.1)$$

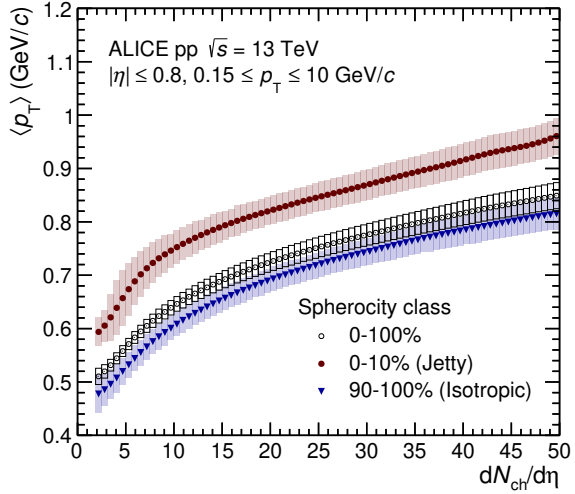


Figure 9.2: TBA.

where $p_{T,i}$ represents the vector of transverse momentum of a particle i and \hat{n} is the event-dependent unit vector that minimises the sum. The sum runs over all charged particles in the event within the detector acceptance.

Previous ALICE measurements⁷ studied characteristics of charged particles in pp collisions and discovered their strong dependence of $\langle p_T \rangle$ on spherocity S_O , which validates the previously discussed motivation. This relationship is shown in Fig. 9.2. Additionally, phenomenological studies of S_O in Pythia 8 further demonstrate its classifying power by finding strong dependence of $\langle n_{MPI} \rangle$ as well as the mean number of reconstructed jets $\langle n_j \rangle$ on S_O ^{??}. These results can be seen in Fig. 9.3.

This work uses a modified definition of this observable, *unweighted* transverse spherocity $S_O^{(p_T=1.0)}$, defined as follows:

$$S_O^{(p_T=1.0)} = \frac{\pi^2}{4} \min_{\hat{n}} \left(\frac{\sum_i |\hat{p}_{T,i} \times \hat{n}|}{N_{trks}} \right)^2 , \quad (9.2)$$

where $\hat{p}_{T,i}$ represents the *unit* vector of transverse momentum of a particle i and N_{trks} the number of charged particles entering the sum.

In this thesis, unless stated otherwise, the terms transverse spherocity and spherocity are both used to refer to this unweighted transverse spherocity $S_O^{(p_T=1.0)}$.

Applying the spherocity $S_O^{(p_T=1.0)}$, events in two geometrical limits can be studied:

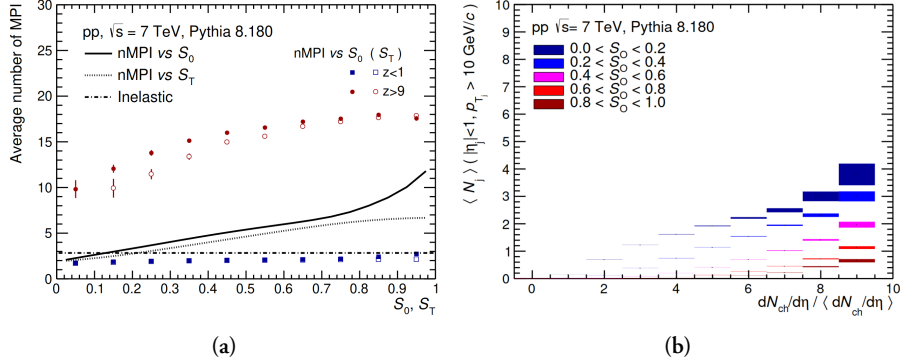


Figure 9.3: TBA.

- $S_O^{(p_T=1.0)} \rightarrow 0$: the “jetty” limit. Pencil-like topology is selected. These events are dominated by hard pQCD processes. In this limit, with perfectly collimated back-to-back particles, \hat{n} coincides with them. Thus, the sum of vector products in Eq. 9.2 contains only zero values as $\sin 0 = \sin \pi = 0$.
- $S_O^{(p_T=1.0)} \rightarrow 1$: the “isotropic” limit. Circular topology is selected. Such events are dominated by multiple softer non-perturbative processes¹. In this limit of $N \rightarrow \infty$ uniformly distributed unit vectors within $(0, 2\pi)$, the choice of \hat{n} becomes arbitrary and calculation of the sum in Eq. 9.2 leads to:

$$\frac{1}{N} \sum_{n=1}^N |\sin \frac{2\pi n}{N}| \approx \frac{1}{N} \int_0^N |\sin \frac{2\pi x}{N}| dx \quad (9.3)$$

$$= \frac{2}{N} \int_0^{N/2} \sin \frac{2\pi x}{N} dx = \frac{1}{\pi} \int_0^\pi \sin u du \quad (9.4)$$

$$= \frac{1}{\pi} [-\cos x]_0^\pi = \frac{2}{\pi} \quad (9.5)$$

and therefore $S_O^{(p_T=1.0)} = 1$.

Figure 9.4 illustrates how spherocity slowly approaches the circular limit value with increasing N compared to other event shape observables. This property makes spherocity favoured by experimentalists in these measurements, as it provides the highest discrimination power of isotropic events?

¹However, it is important to mention that anisotropic collective flow such as v_2 , a non-perturbative phenomenon, reduces the event isotropy.

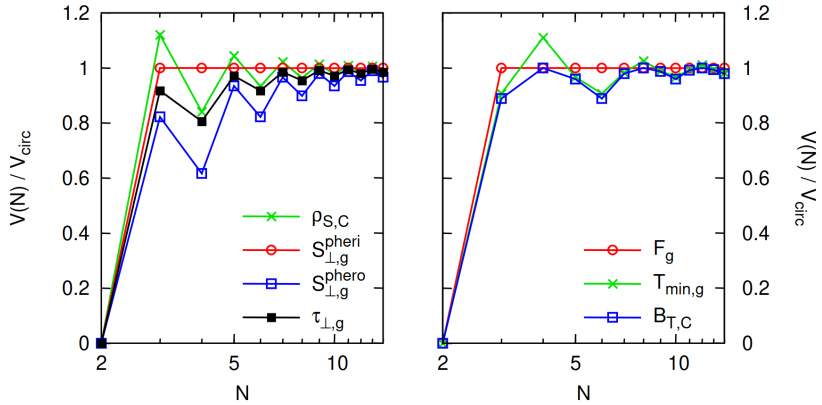


Figure 9.4: TBA.

9.1.3 Relationship between $S_O^{(p_T=1.0)}$ and S_O

In ALICE, only charged particles are considered when calculating spherocities. This introduces biases when measuring charged and neutral species of hadrons. For instance, even topologically identical events with dominant high- p_T leading π^+ and π^0 can yield significantly different values of the traditional p_T -weighted spherocity S_O , despite being comparable in all relevant aspects. In contrast, unweighted spherocity $S_O^{(p_T=1.0)}$ offers a more similar quantification of the two events, as shown in Fig. 9.5. However, it should be noted that this modified definition is only applicable to events with many tracks (i.e., $N_{\text{trks}} > 10$).

In addition, while not a large concern in high-multiplicity collisions? , $S_O^{(p_T=1.0)}$ also offers improved resolution compared to S_O , as the failure to reconstruct a high- p_T track has a smaller impact. Overall, S_O and $S_O^{(p_T=1.0)}$ exhibit similar values and interpretations, with a strong correlation between the two, as illustrated in Fig. 9.6.

9.1.4 Track and event selection

The measurements are carried out on MB events with $\text{INEL} > 0$, requiring at least one hit in the V0A or V0C scintillators and one charged particle reconstructed within $|\eta| < 1$. The primary vertex is reconstructed using hits in the SPD and is required to be within 10 cm of the interaction point. The fast read-out time of the SPD allows rejection of out-of-bunch pile-up. In-bunch pile-up is further removed by excluding events with multiple reconstructed vertices. The presented results are based on high-multiplicity events, selected by the classifiers V0M (forward rapidity) and $N_{\text{tracklets}}^{|\eta| < 0.8}$

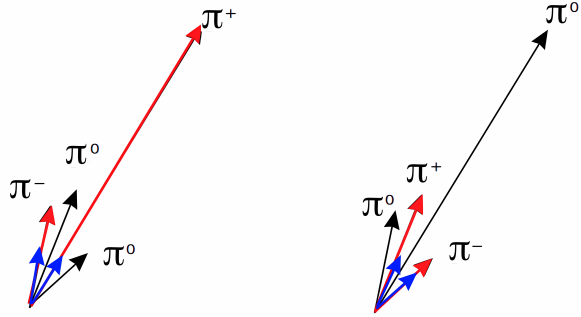


Figure 9.5: TBA.

(mid-rapidity), and require a minimum of 10 reconstructed tracks within $|\eta| < 0.8$ and with $p_T > 0.15 \text{ GeV}/c$.

To ensure a high level of azimuthal acceptance uniformity, which is important for event shape measurements, the following, rather loose, selection criteria are employed:

1. The SPD is not used due to its holes, at the expense of a lower momentum resolution.
2. A track is required to have at least 50 clusters in the TPC and be matched to hits in the ITS to improve tracking precision and further reject pile-up.
3. DCA cuts are applied in both the longitudinal ($|\text{DCA}_z| < 3.2 \text{ cm}$) and transverse ($|\text{DCA}_{xy}| < 2.4 \text{ cm}$) planes to ensure that the reconstructed TPC track points to the primary vertex.

It should be noted that charged decay products of V0s with low p_T ($\lesssim 1 \text{ GeV}/c$) and small decay radius may enter and influence $S_O^{(p_T=1.0)}$ determination.

9.1.5 Multiplicity selection and its interplay with $S_O^{(p_T=1.0)}$

Spherocity exhibits a twofold correlation with multiplicity that is not particularly informative. First, the definition of $S_O^{(p_T=1.0)}$ results in higher values for events with more uniformly distributed particles, as shown in Fig. 9.4. Second, in models such as Pythia, high multiplicity is often associated with more MPI, which tend to lead to higher isotropy due to the increased number of emission sources. To gain a more nuanced understanding of the relationship between spherocity and multiplicity, we

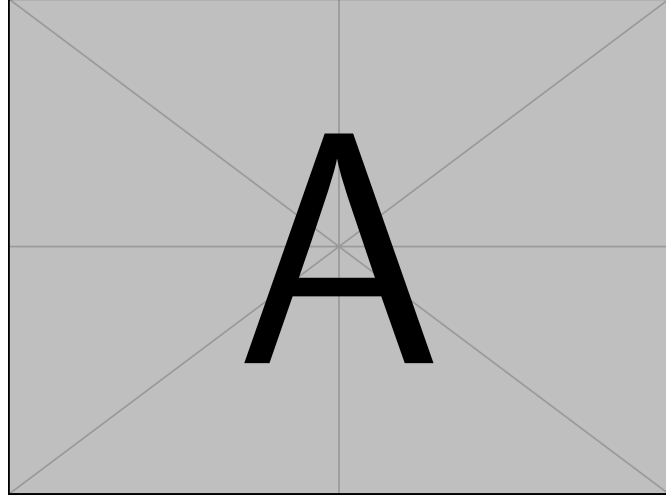


Figure 9.6: TBA.

analyze the effect of $S_O^{(p_T=1.0)}$ on measured particles in high-multiplicity events determined in two distinct rapidity regions, as described above. Specifically, the top 1% (10%) quantiles are used, denoted as V0M I and $N_{\text{SPD}_{\text{Trkts}}} \text{ I}$ ($V0M \text{ I-III}$ and $N_{\text{SPD}_{\text{Trkts}}} \text{ I-III}$).

Figure 9.7 shows the effect of $S_O^{(p_T=1.0)}$ on the pion yields and $\langle p_T \rangle$. Pions are measured in the high-multiplicity events and in top and bottom 10% and 1% quantiles of $S_O^{(p_T=1.0)}$. The result reveals that when measuring multiplicity in forward rapidity (V0M I), the effect of $S_O^{(p_T=1.0)}$ causes a change of approximately 100% in the yields when going from jetty to isotropic limits, whereas the difference in $\langle p_T \rangle$ is only ca. 10%. Conversely, when determining the multiplicity in mid-rapidity ($N_{\text{SPD}_{\text{Trkts}}} \text{ I}$), the same region where the pion spectra are reconstructed, the change in the yields is only approximately 10% while the change in $\langle p_T \rangle$ is ca. 25%.

For this reason, the following combinations of multiplicity and $S_O^{(p_T=1.0)}$ selections are presented:

1. $N_{\text{SPD}_{\text{Trkts}}} \text{ I}$ and $S_O^{(p_T=1.0)}$ top and bottom 10% quantiles: This selection emphasises the impact of extreme event topologies on the QCD processes whilst minimising the effect of multiplicity dependence.
2. $N_{\text{SPD}_{\text{Trkts}}} \text{ I-III}$ and $S_O^{(p_T=1.0)}$ top and bottom 1% quantiles: This selection shows the effect of even more extreme event topologies but with overall less and somewhat varying multiplicity.

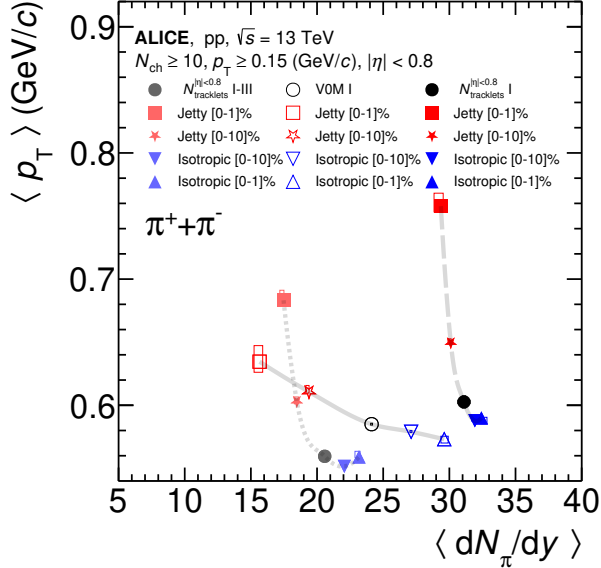


Figure 9.7: TBA.

3. V0M I and $S_O^{(p_T=1.0)}$ top and bottom 10% quantiles: This selection highlights the effect of extreme event topologies with highly varying mid-rapidity multiplicity. It also allows for a comparison with $N_{SPD_{Trkts}}$ I-III and $S_O^{(p_T=1.0)}$ 1% selection, as the mid-rapidity multiplicity and the $\langle p_T \rangle$ variations are more similar.

The mid-rapidity multiplicities in the different high-multiplicity classes are reported in Tab. 9.1. The measured $S_O^{(p_T=1.0)}$ distributions in $N_{SPD_{Trkts}}$ I, $N_{SPD_{Trkts}}$ I-III, and V0M I-III are shown in Fig. 9.8. They are treated with Bayesian unfolding to account for reconstruction effects. They are also compared with theoretical predictions from Pythia 8 (Monash and Ropes tunes), EPOS LHC, and Herwig. Table ?? provides the $S_O^{(p_T=1.0)}$ cut values associated with the quantile selections in data.

Table 9.1: TBA.

Event class	$N_{SPD_{Trkts}}$ I	$N_{SPD_{Trkts}}$ I-III	V0M I
$\langle dN_{\text{ch}}/d\eta \rangle$	33.01 ± 0.55	21.57 ± 0.32	26.02 ± 0.35

Table 9.2: Values of the different quantiles of the uncorrected $S_O^{(p_T=1.0)}$ distribution used for the event selections in this analysis.

Event class	N_{SPDTrkts} I	N_{SPDTrkts} I-III	V0M I
Jetty			
$S_O^{(p_T=1.0)} 0-1\%$	< 0.487	< 0.408	< 0.433
$S_O^{(p_T=1.0)} 0-10\%$	< 0.624	< 0.561	< 0.589
Isotropic			
$S_O^{(p_T=1.0)} 90-100\%$	> 0.892	> 0.871	> 0.882
$S_O^{(p_T=1.0)} 99-100\%$	> 0.942	> 0.930	> 0.936

9.1.6 Comparison of V0 production with MC generators

Further on in this chapter, the results of K_S^0 , Λ , and $\bar{\Lambda}$ as a function of $S_O^{(p_T=1.0)}$ are presented and compared with predictions from phenomenological models Pythia 8, EPOS LHC, and Herwig obtained from MC simulations. To mitigate the effect of reconstruction on the experimental results and make the comparison with these predictions as comparable as possible, the following strategies were employed based on findings using the ALICE MC simulations:

- The results were compared using the same quantiles of the $S_O^{(p_T=1.0)}$ distributions in both the MC and the data, instead of relying on the experimental $S_O^{(p_T=1.0)}$ ranges determined by specific cut values. This approach reduced the effects of $S_O^{(p_T=1.0)}$ resolution.
- In the MC simulations, the $S_O^{(p_T=1.0)}$ calculations included neutral particles K_S^0 , Λ , and $\bar{\Lambda}$, despite their neutral charge. This helped minimize differences between the true and reconstructed/corrected MC results, possible due to the potential contribution of charged V0 daughters to the $S_O^{(p_T=1.0)}$ calculation.

Any discrepancies that still persisted between the true and reconstructed/corrected transverse momentum spectra were accounted for as systematic uncertainties.

9.2 Systematic uncertainties

The systematic uncertainties associated with the p_T spectra of K_S^0 , Λ , and $\bar{\Lambda}$ were evaluated separately for N_{SPDTrkts} I and V0M I events with no $S_O^{(p_T=1.0)}$ selection, as well as for the top and bottom 10% isotropic and jetty quantiles, using the methodology described in Section ???. The relative systematic uncertainties obtained from these

configurations were also applied to the $N_{\text{SPD}_{\text{Trkts}}}$ I-III and V0M I-III event classes with different jetty/isotropic quantiles.

9.2.1 Variations in alternative methods

Figures 9.9, 9.10, and 9.11 illustrate the variations resulting from alternative cut values, extraction parameters, or feeddown methods in V0M I, $S_O^{(p_T=1.0)}$ -unbiased events for K_S^0 , Λ , and $\bar{\Lambda}$, respectively. The maximal deviations, contributing to the final systematic uncertainties, are also shown.

9.2.2 Experimental bias

TBA

9.2.3 Correlation of uncertainties with $S_O^{(p_T=1.0)}$

Correlations of several systematic uncertainties with respect to the $S_O^{(p_T=1.0)}$ selection are expected. Since the ratios of jetty/isotropic results to $S_O^{(p_T=1.0)}$ -unbiased ones provide important insights, it is necessary to study and account for these correlations.

TBA add methodology.

The systematic uncertainty associated with the material budget is fully correlated, while assuming the reconstruction efficiency is independent of multiplicity leads to an uncorrelated uncertainty. This assumption would lead to a factor of $\sqrt{2}$ in the ratios of jetty/isotropic to $S_O^{(p_T=1.0)}$ -unbiased for this uncertainty. However, in ALICE, this assumption is generally considered too conservative by ALICE, and thus this factor is dropped. The same approach is used for the uncertainty associated with the multiplicity independence of the feeddown matrix. Detailed results can be found in Appendix ??.

9.2.4 Summary

The total systematic uncertainties are reported in Tab. 9.3 and visualised in Fig. 9.12.

Table 9.3: The most relevant systematic uncertainties for the long-lived particles K_S^0 and Λ ($\bar{\Lambda}$) as a function of $S_O^{(p_T=1.0)}$. “HM” in this table represents the $S_O^{(p_T=1.0)}$ -unbiased spectra. Uncertainties are p_T -dependent, and the ranges listed represents the minimum-maximum values presented in the final spectra (see text for details).

Topology:	Jetty	Iso	HM	Jetty/HM	Iso/HM
K_S^0					
Selection cuts	3%	3–4%	3–4%	Negl.	1%
Track pile-up	1%	1–3%	1%	0–2%	0–2%
Signal extraction	1–3%	1–3%	1–3%	Negl.	Negl.
Efficiency	2%	2%	2%	2%	2%
Material budget	4%	4%	4%	—	—
Experimental bias	4%	1%	—	4%	1%
Total uncertainty	7%	6–7%	5–6%	5%	2–3%
$\Lambda(\bar{\Lambda})$					
Selection cuts	1–5%	2–6%	4–5%	0–1%	0–3%
Track pile-up	4–5%	5%	3–5%	0–1.5%	0–1%
Signal extraction	2–6%	2–6%	2–6%	0–2%	0–1%
Feed-down correction	1.0–1.5%	1.0–1.5%	1.0–1.5%	Negl.	Negl.
Efficiency	2%	2%	2%	2%	2%
Material budget	4%	4%	4%	—	—
Experimental bias	4%	1%	—	4%	1%
Total uncertainty	8–10%	8–9%	7–9%	5%	3–4%

9.3 Transverse momentum spectra vs. $S_O^{(p_T=1.0)}$

The corrected spectra in V0M and $N_{\text{SPD}_{\text{Trkts}}}$ high-multiplicity events and the dependence on spherocity for the K_S^0 and $\Lambda + \bar{\Lambda}$ can be seen in Fig. 9.13 and Fig. 9.14, respectively.

9.4 Ratios to pions

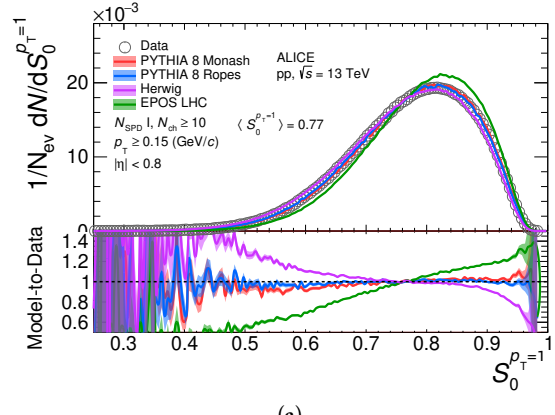
TBA plots and discussion

9.5 Baryon-to-meson ratio

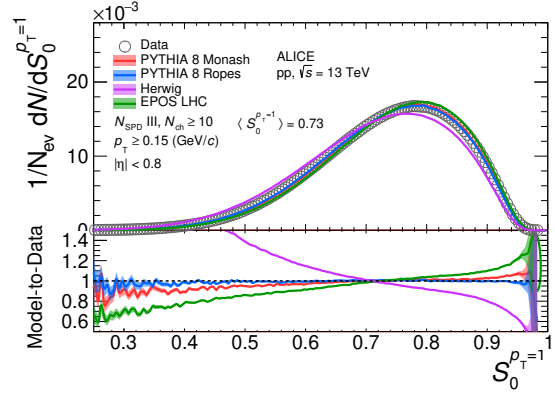
TBA plots and discussion

9.6 Ratio of integrated yields

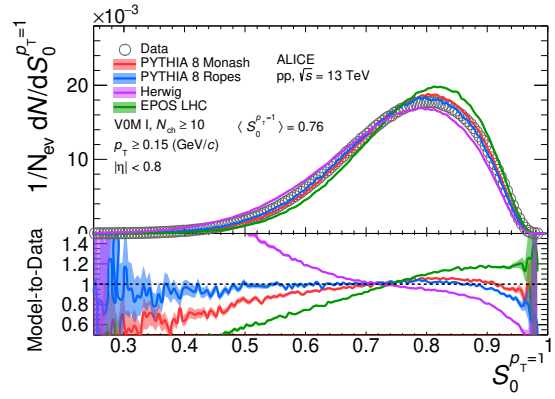
TBA discussion



(a)



(b)



(c)

Figure 9.8: The measured and fully corrected $S_0^{(p_T=1.0)}$ distributions for both (a) $N_{\text{SPD}} = 0-1\%$, (b) $0-10\%$ and (c) VOM $0-1\%$. The curves represent different model prediction, where the shaded area represents the statistical uncertainty of the models.

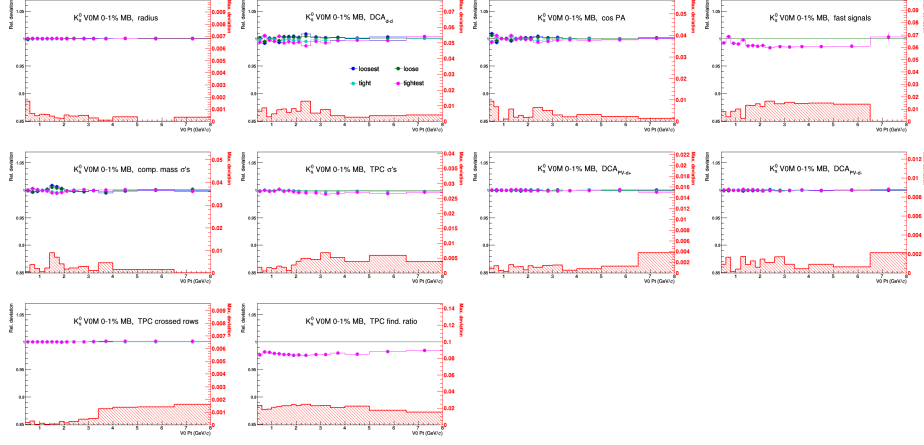


Figure 9.9: Deviations of the corrected spectra w.r.t. the different cut variations used for the K_S^0 . The maximum deviation is added in quadrature to the total, if it's larger than σ_{RB} (depicted as errorbars) from unity.

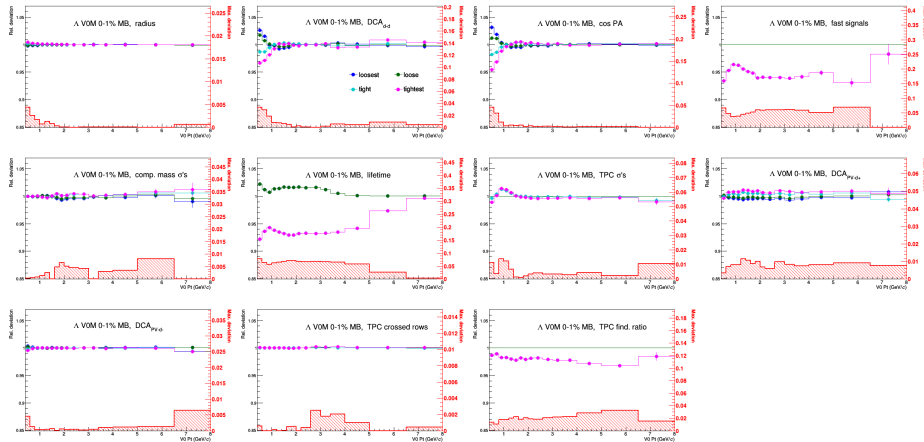


Figure 9.10: Deviations of the corrected spectra w.r.t. the different cut variations used for the K_S^0 . The maximum deviation is added in quadrature to the total, if it's larger than σ_{RB} (depicted as errorbars) from unity.

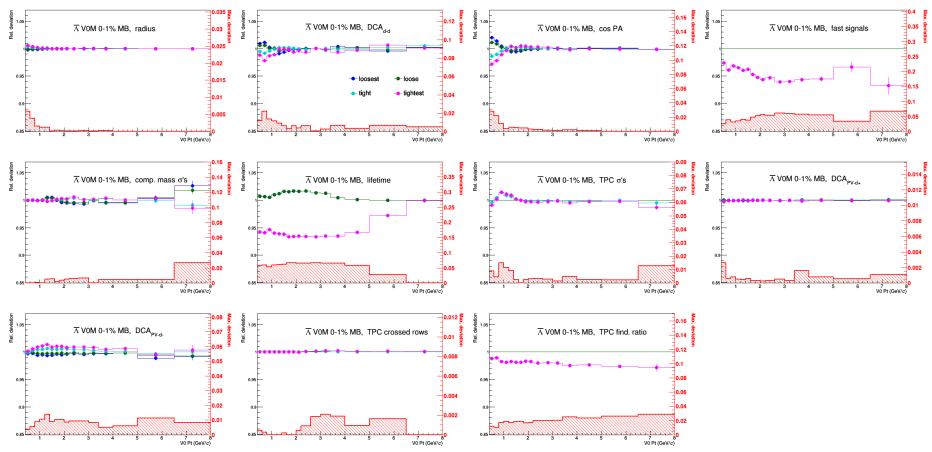
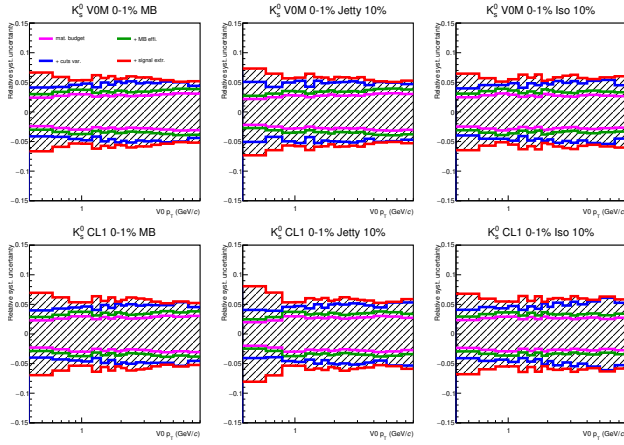
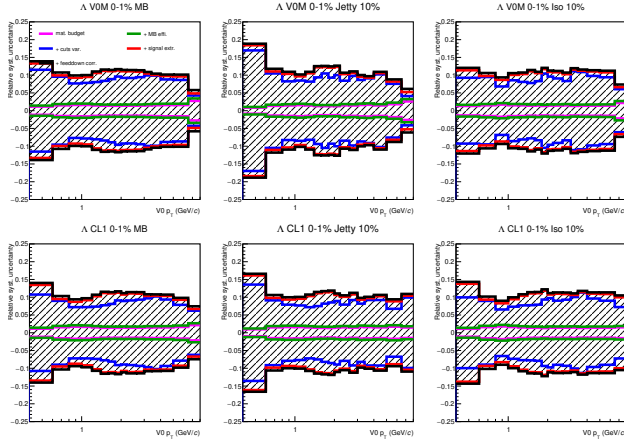


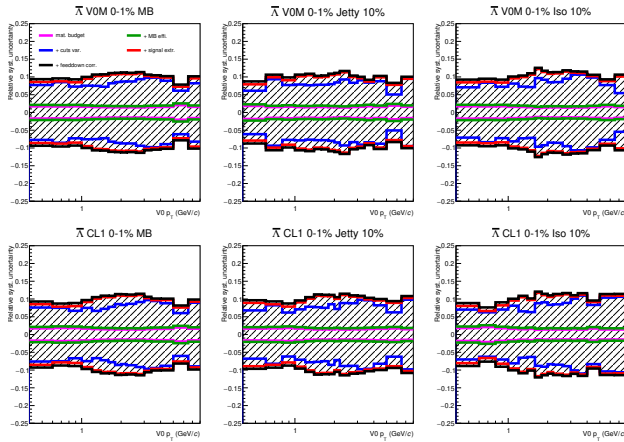
Figure 9.11: Deviations of the corrected spectra w.r.t. the different cut variations used for the K_S^0 . The maximum deviation is added in quadrature to the total, if it's larger than σ_{RB} (depicted as errorbars) from unity.



(a)



(b)



(c)

Figure 9.12: Total relative systematic uncertainty and individual contributions for the K_s^0 , Λ , and $\bar{\Lambda}$.

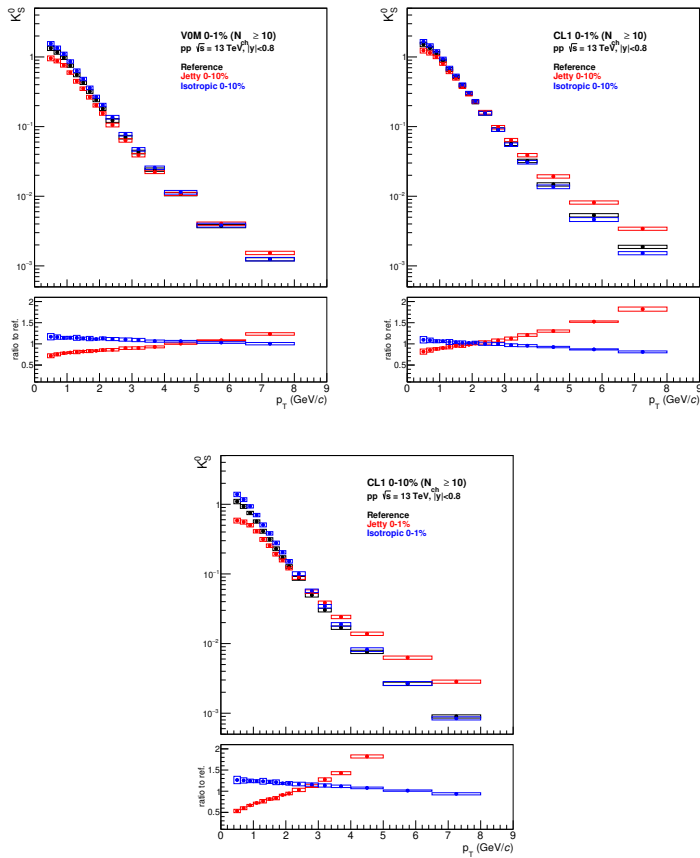


Figure 9.13: Corrected and normalised p_T -spectra of the K_S^0 particle in high-multiplicity V0M 0-1% (top left), CL1 0-1% (top middle, bottom right), and CL1 0-10% (top right) events, shown as black points. The bottom (jetty) and top (isotropic) 1% or 10% of spherocity events are also shown as red and blue points. The ratios of isotropic/jetty spectra to the high-multiplicity spectra are shown in the bottom panels.

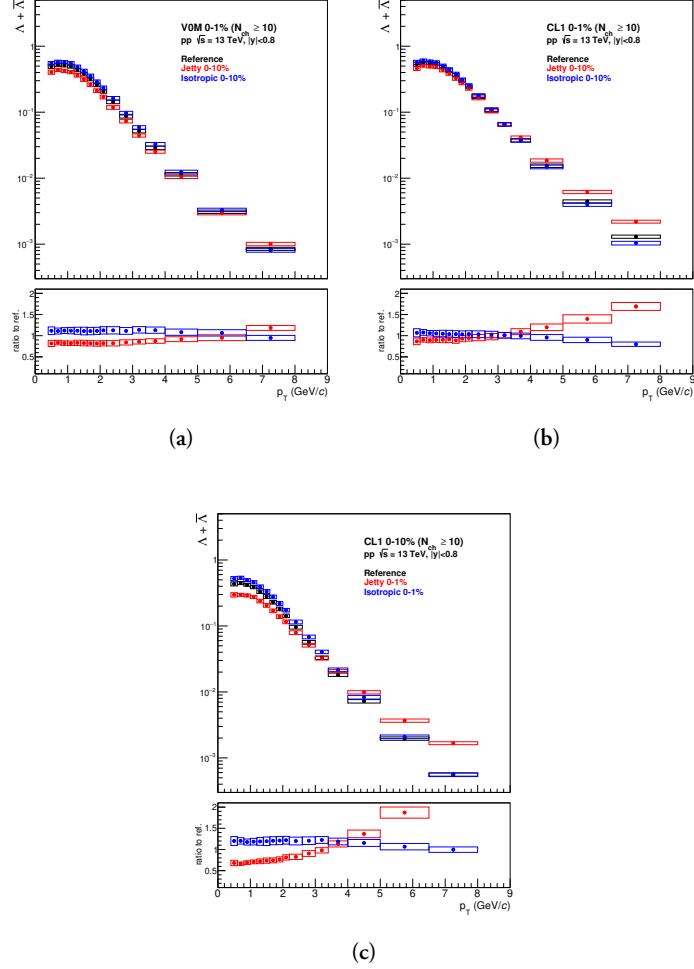


Figure 9.14: Corrected and normalised p_T -spectra of the $\Lambda + \bar{\Lambda}$ particles in high-multiplicity VOM 0-1% (top left, bottom left), CL1 0-1% (top middle, bottom right), and CL1 0-10% (top right) events, shown as black points. The bottom (jetty) and top (isotropic) 1% or 10% of spherocity events are also shown as red and blue points. The ratios of isotropic/jetty spectra to the high-multiplicity spectra are shown in the bottom panels.

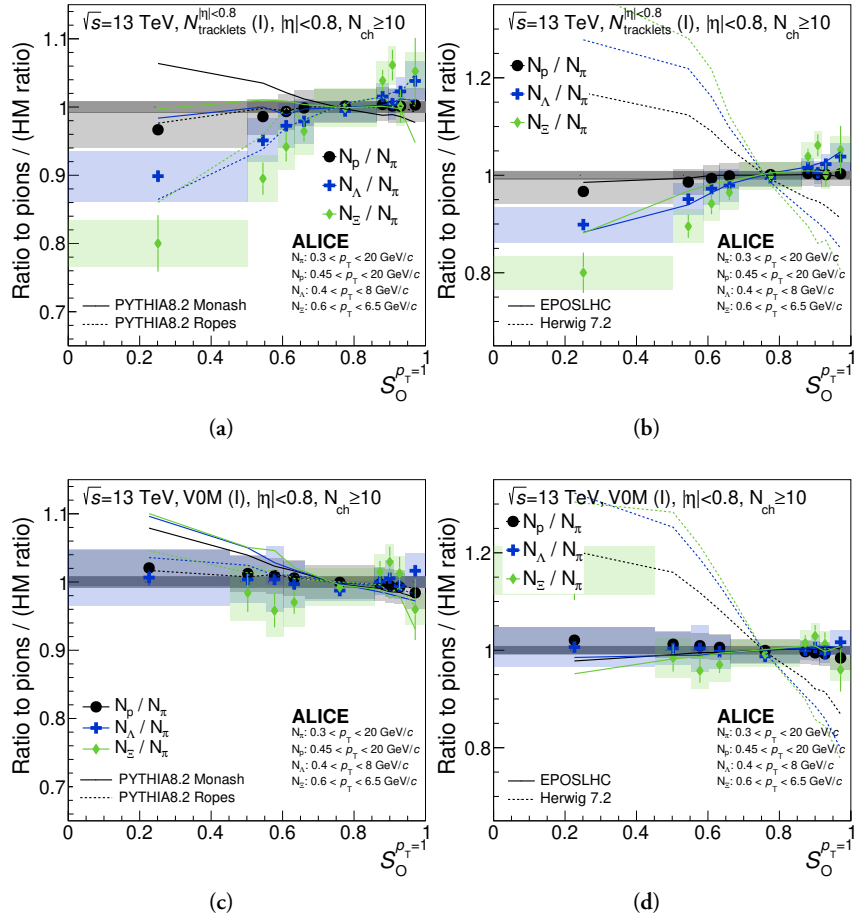


Figure 9.15: TBA.